REPORT DOCUMENTATION PAGE

Form Approved
OMB No. 0704-0188

PLEASE DO NOT RETURN YOUR FORM TO THE ABOVE ORGANIZATION.

1. REPORT DATE *(DD-MM-YYYY)*	2. REPORT TYPE	3. DATES COVERED *(From - To)*
23 Mar 2008	FINAL REPORT	01 May 2007 - 31 Dec 2007

4. TITLE AND SUBTITLE

DEMONSTRATON OF A HIGH-REJECTION/LOW-LOSS X-BAND TUNABLE NOTCH FILTER FOR CO-SITE INTERFERENCE MITIGATION ON AIRBORNE PLATFORMS

5a. CONTRACT NUMBER

FA9550-07-1-0409

5b. GRANT NUMBER

5c. PROGRAM ELEMENT NUMBER

6. AUTHOR(S)

KAMAL SARABANDI

5d. PROJECT NUMBER

5e. TASK NUMBER

5f. WORK UNIT NUMBER

7. PERFORMING ORGANIZATION NAME(S) AND ADDRESS(ES)

UNIVERSITY OF MICHIGAN

8. PERFORMING ORGANIZATION REPORT NUMBER

9. SPONSORING/MONITORING AGENCY NAME(S) AND ADDRESS(ES)

KITT REINHARDT
AF OFFICE OF SCIENTIFIC RESEARCH
875 NORTH RANDOLPH STREET ROOM 3112
ARLINGTON VA 22203

10. SPONSOR/MONITOR'S ACRONYM(S)

11. SPONSOR/MONITOR'S REPORT NUMBER(S)

AFRL-SR-AR-TR-08-0268

12. DISTRIBUTION/AVAILABILITY STATEMENT

DISTRIBUTION STATEMENT A: UNLIMITED

13. SUPPLEMENTARY NOTES

14. ABSTRACT

A low loss 4-6 GHz 3-bit tunable filter was designed and fabricated on a quartz substrate. A high-Q 3-bit orthogonal RF-MEMS capacitance network is presented and its significance on the filter Q is discussed. Detailed design equations for the capacitively-loaded coupled open-loop ¸=2 resonators and realization of capacitive external coupling with source-load impedance loading are discussed. The measured filter shows an unloaded-Q of 85-170, an insertion loss of 1.5-2.8 dB (including connector loss), and the measured 1-dB bandwidth is 4.35 § 0.35% over the 4-6 GHz tuning range. The measured IIP3 and 1-dB power compression point at 5.91 GHz are > 40 dBm and 27.5 dBm, respectively. The unloaded Q and insertion loss can be improved to 125-210 and 1.8-1.1 dB with the use of a thicker bottom electrode. To our knowledge, this is the highest Q tunable planar filter to-date at this frequency range.

15. SUBJECT TERMS

RF-MEMS, capacitance network, coupled openloop resonators, capacitive loading, tunable filter, source-load impedance loading

16. SECURITY CLASSIFICATION OF:			17. LIMITATION OF ABSTRACT	18. NUMBER OF PAGES	19a. NAME OF RESPONSIBLE PERSON
a. REPORT	b. ABSTRACT	c. THIS PAGE		14	19b. TELEPHONE NUMBER *(Include area code)*

Reset

Standard Form 298 (Rev. 8/98)
Prescribed by ANSI Std. Z39.18

Low-Loss 4-6 GHz Tunable Filter With 3-Bit High-Q Orthogonal RF-MEMS Capacitance Network

Sang-June Park, *Student Member, IEEE,* Mohammed A. El-Tanani, *Student Member, IEEE,* Isak Reines, *Student Member, IEEE,* and Gabriel M. Rebeiz, *Fellow, IEEE*

***Abstract*— A low loss 4-6 GHz 3-bit tunable filter was designed and fabricated on a quartz substrate. A high-Q 3-bit orthogonal RF-MEMS capacitance network is presented and its significance on the filter Q is discussed. Detailed design equations for the capacitively-loaded coupled open-loop $\lambda/2$ resonators and realization of capacitive external coupling with source-load impedance loading are discussed. The measured filter shows an unloaded-Q of 85-170, an insertion loss of 1.5-2.8 dB (including connector loss), and the measured 1-dB bandwidth is 4.35 $\pm$ 0.35% over the 4-6 GHz tuning range. The measured IIP3 and 1-dB power compression point at 5.91 GHz are $>$ 40 dBm and 27.5 dBm, respectively. The unloaded Q and insertion loss can be improved to 125-210 and 1.8-1.1 dB with the use of a thicker bottom electrode. To our knowledge, this is the highest Q tunable planar filter to-date at this frequency range.**

***Index Terms*— RF-MEMS, capacitance network, coupled open-loop resonators, capacitive loading, tunable filter, source-load impedance loading.**

I. Introduction

Low-loss tunable filters are essential for modern wide-band communication systems. Most of them can be classified in three categories; YIG filters [1], varactor diode filters [2]–[4], and RF-MEMS filters [5]–[8]. The YIG filters have muti-octave tuning ranges and a Q up to 10,000, however, their power consumption, tuning speed, size, and weight limit their use in highly integrated communication systems. The varactor diode tuned filters are small in size and with ns tuning speed, but their loss, low power handling, and low IP3 values have been limiting factors for their use in wireless systems. The RF-MEMS tunable filters occupy a sweet spot between YIG and Schottky-diode filters in terms of being planar and physically small and have zero power consumption, μs tuning speeds and excellent linearity (IP3¿40 dBm) [9].

The RF-MEMS tunable filters reported so far have an estimated Q of 20-150 [5]–[8]. The filter Q is usually 30-80 except for a narrow band switchable case as demonstrated by Park $et.al$ [8]. The filter Q has been quite low even though the MEMS device itself has a $Q > 250$ at the design frequency [10]. In the previous RF-MEMS tunable filters, the loss mechanisms of the multi-bit capacitance tuing network have not been investigated intensively and will be shown in this paper, this can have a large effect on the filter loss and Q.

In this work, the loss mechanisms of the multi-bit capacitance network are analyzed and a novel orthogonal capacitance network design is introduced as a solution. A distributed coupled resonator design using admittance matrix is presented and this is rewritten instead of using a symmetry image plane [8] by calculating the loading capacitance directly from the admittance matrix. The matching capacitance and modified loading capacitance calculation are also rewritten by including the source and load impedance in the admittance matrix. A design method for the orthogonal capacitance network to achieve uniform step coverage in the frequency response is also presented in detail. These design methods are applied on a capacitively-loaded 2-pole 4-6 GHz tunable filter with 3-bit frequency control (8 states) to achieve state-of-the-art performance.

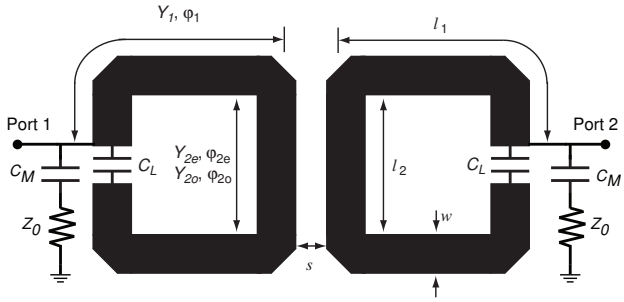

Fig. 1. Electrical circuit model of the coupled-resonator filter with 2 ports.

II. Design

A. Filter Admittance Matrix With Source-Load Impedance Loading

The admittance matrix of the coupled resonators with the loading capacitors, C_L, without the matching capacitors, C_M, and source-load impedance, Z_0, in Fig. 1 is [8]

This work was supported by US-AFRL under contract number FA8718-04-C-0029, Jack Ebel and Eric Marsh, contract monitors.

Sang-June Park is with the Radiation Laboratory, Department of Electrical Engineering and Computer Science, University of Michigan (e-mail: sangjp@umich.edu).

Gabriel M. Rebeiz is with the Department of Electrical and Computer Engineering, University of California, San Diego (email: rebeiz@ece.ucsd.edu).

Mohammed A. El-Tanani is with the Department of Electrical and Computer Engineering, University of California, San Diego (email: mtanani@ucsd.edu).

Isak Reines is with the Department of Electrical and Computer Engineering, University of California, San Diego (email: ireines@ece.ucsd.edu).

$$Y_r = \begin{bmatrix} \frac{Y_{in\_e}+Y_{in\_o}}{2} & \frac{Y_{in\_e}-Y_{in\_o}}{2} \\ \frac{Y_{in\_e}-Y_{in\_o}}{2} & \frac{Y_{in\_e}+Y_{in\_o}}{2} \end{bmatrix} \quad (1)$$

where

$$Y_{in\_e} = \frac{(c_e-1)(c_e+1-2d_e\omega C_L)}{j(c_e d_e - d_e^2\omega C_L)} \quad (2)$$

$$Y_{in\_o} = \frac{(c_o-1)(c_o+1-2d_o\omega C_L)}{j(c_o d_o - d_o^2\omega C_L)} \quad (3)$$

$$c_{e,o} = \cos 2\phi_1 \cos\phi_{2e,o} - \frac{1}{2}\left(\frac{Y_{2e,o}}{Y_1} + \frac{Y_1}{Y_{2e,o}}\right)\sin 2\phi_1 \sin\phi_{2e,o} \quad (4)$$

$$d_{e,o} = \frac{\sin 2\phi_1}{Y_1}\cos\phi_{2e,o} + \left(\frac{\cos^2\phi_1}{Y_{2e,o}} - \frac{Y_{2e,o}\sin^2\phi_1}{Y_1^2}\right)\sin\phi_{2e,o}. \quad (5)$$

The overall admittance matrix of the filter in Fig. 1 with C_M, and the source-load impedance (Z_0) is

$$Y = \begin{bmatrix} Y_{r11} + \frac{j\omega C_M}{1+Z_0 j\omega C_M} & Y_{r12} \\ Y_{r12} & Y_{r11} + \frac{j\omega C_M}{1+Z_0 j\omega C_M} \end{bmatrix} \quad (6)$$

where

$$Y_{r11} = \frac{Y_{in\_e}+Y_{in\_o}}{2}, \quad Y_{r12} = \frac{Y_{in\_e}-Y_{in\_o}}{2}. \quad (7)$$

B. Filter Design Using Admittance Matrix Method

1) Realizing the coupling section of the filter: The coupling section of the filter can be realized using the following coupling condition. The condition is

$$\frac{Im[Y_{r12}(\omega_0)]}{b} = k_{12} \quad (8)$$

where

$$b_r = \frac{\omega_0}{2}\frac{\partial Im[Y_{r11}(\omega_0)]}{\partial\omega}, \quad k_{12} = \frac{\Delta}{\sqrt{g_1 g_2}}. \quad (9)$$

The slope parameter, b_r, is a function of the design parameters, Y_1, $Y_{2e,o}$, ϕ_1, $\phi_{2e,o}$ and loading capacitor C_L. However, it is required to decouple C_L from b_r so that one can obtain design parameters independent of C_L and leave C_L as a frequency tuning parameter. From the resonance condition, $Im[Y_{r11}(\omega_0)] = 0$, C_L can be rewritten as

$$C_L = \frac{-B(\omega_0) + \sqrt{B(\omega_0)^2 - 4A(\omega_0)D(\omega_0)}}{2\omega_0 A(\omega_0)} \quad (10)$$

where

$$A = 2d_o^2 d_e(c_e-1) + 2d_e^2 d_o(c_o-1) \quad (11)$$

$$B = -2d_o d_e(2c_o c_e - c_o - c_e) - d_o^2(c_e^2-1) - d_e^2(c_o^2-1) \quad (12)$$

$$D = c_o d_o(c_e^2-1) + c_e d_e(c_o^2-1). \quad (13)$$

with C_L replaced with (10) in b_r and Y_{r12}, the left-hand side of (8) becomes only a function of the design parameters. By choosing the design parameters satisfying (8), the filter coupling section can be completed.

2) Loading and matching capacitor values with source-load impedance loading: Fig. 1 shows a complete filter circuit with external coupling elements. When the filter external circuit is realized using a reactive element, one finds that its resonance frequency is shifted due to the complex loading effect of the source-load impedance. To take this complex loading effect into account, the admittance matrix of the complete filter circuit, Y, needs to be used to obtain accurate values of the loading capacitor, C_L, and matching capacitor, C_M.

The value of C_L in (10) does not result in the correct resonance frequency (ω_0) when C_M is present. The modified value of C_L and C_M are found by solving the resonance and external coupling conditions, respectively, using (6) as,

$$Im[Y_{11}(\omega_0)] = 0 \quad (14)$$

$$\frac{b}{Re[Y_{11}(\omega_0)]} = Q_{ext} \quad (15)$$

where

$$b = \frac{\omega_0}{2}\frac{\partial Y_{r11}(\omega_0)}{\partial\omega} + \frac{\omega_0}{2}\frac{C_M(1-Z_0^2\omega_0^2C_M^2)}{(1+Z_0^2\omega_0^2C_M^2)^2} \quad (16)$$

$$Q_{ext} = \frac{g_0 g_1}{\Delta}. \quad (17)$$

The b and $Re[Y_{11}(\omega_0)]$ include both C_L and C_M and need to be simplified to a function containing only one of them. C_M can be replaced with an equation in terms of $Y_{r11}(\omega_0)$ (function of C_L only) using (14). C_M with respect to $Y_{r11}(\omega_0)$ is

$$C_M = \frac{-1+\sqrt{1-4B_{11}^2Z_0^2}}{2B_{11}Z_0^2} \quad (18)$$

where

$$B_{11} = Im[Y_{r11}(\omega_0)]. \quad (19)$$

By replacing C_M using (18), the left-hand side of the (15) becomes a function of only C_L, and C_L can be solved using (15). C_M is then determined using (18).

C. Low-Loss Orthogonal Capacitance Network

As is well known, RF-MEMS capacitance networks require high resistance bias lines to actuate the MEMS switches. When multiple bits are realized, the bias lines in the capacitance network couples to the the RF signal and result in additional losses [7].

The effect of the resonant electric field coupled to the bias lines has not been emphasized adequately, but it has significant effect on filter Q. To examine the effects of the resonant electric field in the resonator gap on the bias lines, a 90 MHz butterworth filter centered at 5.95 GHz was simulated

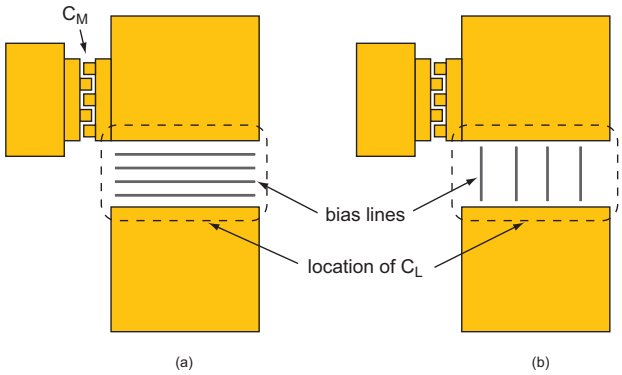

Fig. 2. The orthogonal (a) and parallel (b) (to the electric field) configuration of the bias lines.

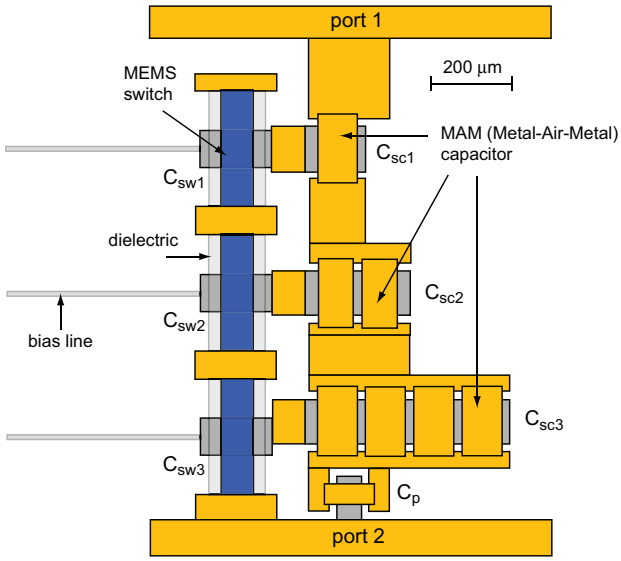

Fig. 3. The low-low 3-bit C_L orthogonal capacitance network (figure is to scale).

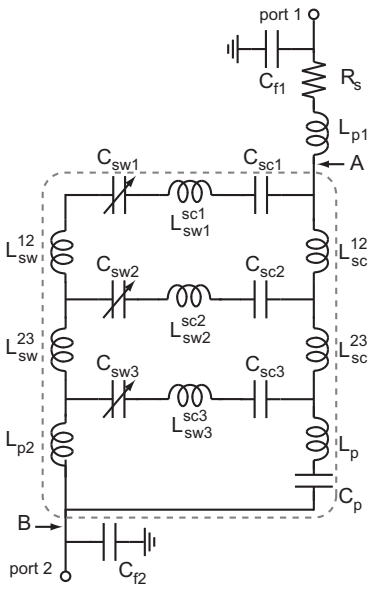

Fig. 4. The equivalent circuit model of the low-low 3-bit C_L capacitance network.

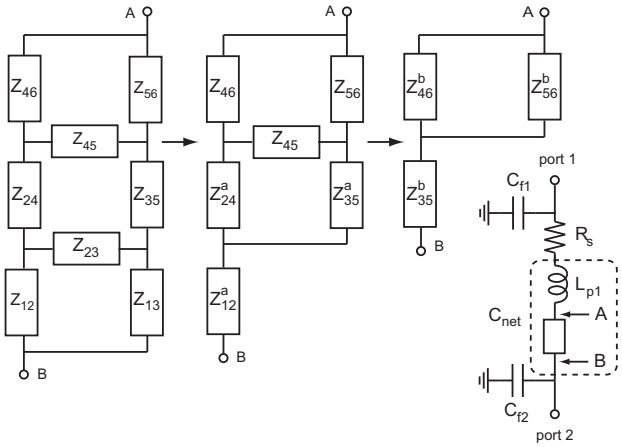

Fig. 5. The Δ-Y transformation to calculate the net capacitance values of the 3-bit C_L capacitance network.

with the two different bias-line configurations (Fig. 2). In this simulation, 5 μm bias line width and 1 kΩ/sq bias line resistance were assumed. The results indicate significantly different pass-band insertion losses. The orthogonal bias-line configuration in Fig. 2(a) has almost identical loss (1.08 dB) as the filter without bias lines (1.07 dB) and is independent of the bias line resistance. On the other hand, the parallel bias-line configuration in Fig. 2(b) results in 5.14 dB and 1.63 dB insertion loss for 1 kΩ/sq and 10 kΩ/sq. bias-line sheet resistance, respectively. It is therefore highly desirable to place the bias lines orthogonal to and as far away as possible from the high electric field area. The suggested *orthogonal* capacitance network in Fig. 3 meets all those requirements.

The equivalent circuit is given in Fig. 4. Each MEMS switch, C_{sw}, is in series with the scaling capacitor C_{sc} and the C_{sw}-C_{sc} series pairs are all connected in parallel. C_p is used to adjust the overall reactance level of the network and C_f is to take into account the fringing capacitance of port 1 and 2.

The net capacitance value of this network is obtained by calculating the total reactance values. The impedances of the network in Fig. 4 are represented in Fig. 5 as:

$$Z_{12} = j\omega L_{p2}, \quad Z_{24} = j\omega L_{sw}^{23} \tag{20}$$

$$Z_{35} = j\omega L_{sc}^{23}, \quad Z_{56} = j\omega L_{sc}^{12} \tag{21}$$

$$Z_{13} = j\omega L_p + \frac{1}{j\omega C_p} \tag{22}$$

$$Z_{23} = j\omega L_{sw3}^{sc3} + \frac{1}{j\omega C_{sw3}} + \frac{1}{j\omega C_{sc3}} \tag{23}$$

$$Z_{45} = j\omega L_{sw2}^{sc3} + \frac{1}{j\omega C_{sw2}} + \frac{1}{j\omega C_{sc2}} \tag{24}$$

$$Z_{46} = j\omega L_{sw}^{12} + j\omega L_{sw1}^{sc1} + \frac{1}{j\omega C_{sw1}} + \frac{1}{j\omega C_{sc1}}. \tag{25}$$

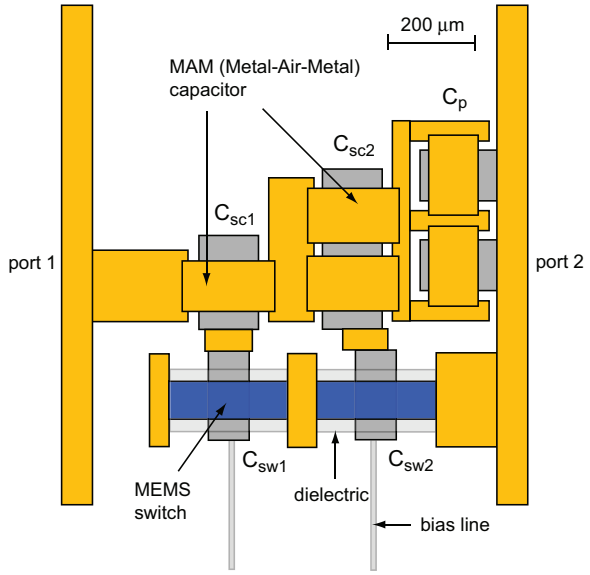

Fig. 6. The low-low 3-bit C_M orthogonal capacitance network (figure is to scale).

After performing the first Δ-Y transformations (Fig. 5), the impedance values are

$$Z_{12}^a = \frac{Z_{12}Z_{13}}{Z_{12}+Z_{13}+Z_{23}} \tag{26}$$

$$Z_{24}^a = \frac{Z_{12}Z_{23}}{Z_{12}+Z_{13}+Z_{23}} + Z_{24} \tag{27}$$

$$Z_{35}^a = \frac{Z_{23}Z_{13}}{Z_{12}+Z_{13}+Z_{23}} + Z_{35}. \tag{28}$$

A second transformation results in

$$Z_{35}^b = Z_{12}^a + \frac{Z_{24}^a Z_{35}^a}{Z_{24}^a+Z_{45}+Z_{35}^a} \tag{29}$$

$$Z_{46}^b = \frac{Z_{24}^a Z_{45}}{Z_{24}^a+Z_{45}+Z_{35}^a} + Z_{46} \tag{30}$$

$$Z_{56}^b = \frac{Z_{45}Z_{35}^a}{Z_{24}^a+Z_{45}+Z_{35}^a} + Z_{56}. \tag{31}$$

The total impedance of the network is therefore

$$Z_{tot} = Z_{35b} + \frac{Z_{46b}Z_{56b}}{Z_{46b}+Z_{56b}} + j\omega L_{p1} + R_s. \tag{32}$$

Finally, the total net capacitance value of the capacitance network is

$$C_{net} = \frac{1}{\omega} Im\left[\frac{1}{Z_{tot}}\right]. \tag{33}$$

If the fringing capacitance, C_f, is not negligible, it can be added to the above result, and the additional capacitance is C_{f1} in series with C_{f2} due to the differential voltage mode at resonance.

The matching capacitance, C_M, is realized using the same concept as C_L and the layout is shown in Fig. 6. The calculation of the net capacitance value also follows the same approach.

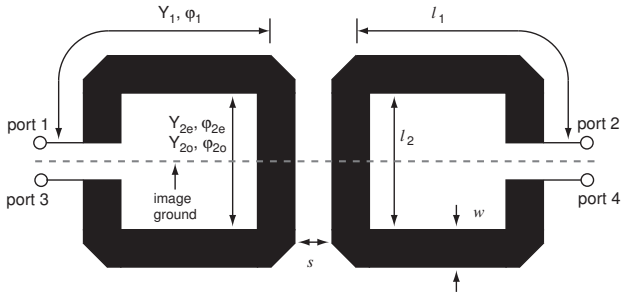

Fig. 7. Electrical circuit model of the balanced coupled-resonator with 4 ports.

III. Implementation of the 4-6 GHz Tunable Filter

To design the 4-6 GHz filter, a full-wave simulation of the coupled resonator structure in Fig. 7 (without capacitors) is performed using Sonnet [11] and the 4-port Y-parameters are extracted. The full-wave 4-port Y-matrix are

$$Y^{4p} = \begin{bmatrix} Y_{11}^{4p} & Y_{12}^{4p} & Y_{13}^{4p} & Y_{14}^{4p} \\ Y_{12}^{4p} & Y_{11}^{4p} & Y_{14}^{4p} & Y_{13}^{4p} \\ Y_{13}^{4p} & Y_{14}^{4p} & Y_{11}^{4p} & Y_{12}^{4p} \\ Y_{14}^{4p} & Y_{13}^{4p} & Y_{12}^{4p} & Y_{11}^{4p} \end{bmatrix}. \tag{34}$$

Calculation of the loading capacitance value giving resonance are simpler if the symmetrical properties of this structure are used [8]. The 2-port Y-parameters of the coupled resonator structure with the image ground plane and the loading capacitance, C_{Ls}, between the port and image ground plane is

$$Y^{2p} = \begin{bmatrix} Y_{11}^{4p} - Y_{13}^{4p} + j\omega C_{Ls} & Y_{12}^{4p} - Y_{14}^{4p} \\ Y_{12}^{4p} - Y_{14}^{4p} & Y_{11}^{4p} - Y_{13}^{4p} + j\omega C_{Ls} \end{bmatrix}. \tag{35}$$

and the loading capacitance, C_{Ls}, which results in the resonance, $Y_{11}^{2p} = 0$, is

$$C_{Ls} = -Im\left[\frac{Y_{11}^{4p}(\omega_0) - Y_{13}^{4p}(\omega_0)}{\omega_0}\right]. \tag{36}$$

The slope parameter of this symmetric network, b^{2p} is

$$b^{2p} = \frac{\omega_0}{2}\frac{\partial Im[Y_{11}^{4p}(\omega_0) - Y_{13}^{4p}(\omega_0)]}{\partial\omega} - \frac{Im[Y_{11}^{4p}(\omega_0) - Y_{13}^{4p}(\omega_0)]}{2} \tag{37}$$

and k_{12} is

$$k_{12} = \frac{Im[Y_{12}^{2p}(\omega_0)]}{b^{2p}} = \frac{\Delta}{\sqrt{g_1 g_2}}. \tag{38}$$

Determining the coupling of the filter can be done by finding a full-wave simulation set satisfying (38) and the loading capacitance, C_{Ls}, is then given by (36).

To complete the design with C_M and the modified C_L, the 2-port full-wave Y-parameters in Fig. 1 without C_M and source-load loading need to be calculated. The 2-port full-wave matrix is obtained by inserting C_L between ports 1 and

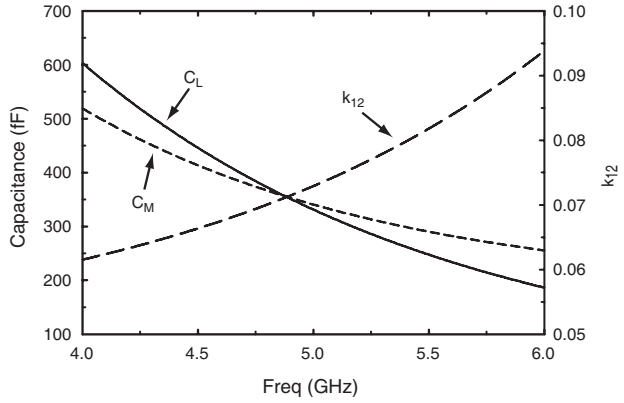

Fig. 8. The loading capacitor, C_L, matching capacitor, C_M, and coupling coefficient, k_{12}, obtained using full-wave simulations.

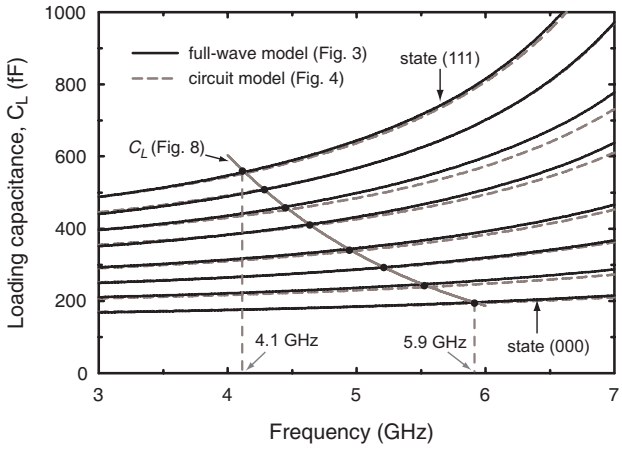

Fig. 9. The calculated C_L using the full-wave simulation of the actual structure in Fig. 3, and the circuit model in Fig. 4.

3 and ports 2 and 4 of the 4-port full-wave matrix and open-circuiting ports 3 and 4. The 2-port full-wave Y-matrix is

$$Y_f = \begin{bmatrix} Y_{f11} & Y_{f12} \\ Y_{f12} & Y_{f11} \end{bmatrix} \tag{39}$$

and the Y_{f11} and Y_{f12} are

$$Y_{f11} = Y_{b11}^{4p} - \frac{Y_{b11}^{4p}[(Y_{b13}^{4p})^2 + (Y_{14}^{4p})^2] - 2Y_{12}^{4p}Y_{b13}^{4p}Y_{14}^{4p}}{(Y_{b11}^{4p})^2 - (Y_{12}^{4p})^2} \tag{40}$$

$$Y_{f12} = Y_{12}^{4p} - \frac{2Y_{b11}^{4p}Y_{b13}^{4p}Y_{14}^{4p} - Y_{12}^{4p}[(Y_{b13}^{4p})^2 + (Y_{14}^{4p})^2]}{(Y_{b11}^{4p})^2 - (Y_{12}^{4p})^2} \tag{41}$$

where

$$Y_{b11}^{4p} = Y_{11}^{4p} + j\omega C_L, \quad Y_{b13}^{4p} = Y_{13}^{4p} - j\omega C_L. \tag{42}$$

The modified C_L and C_M values are then calculated using the method explained in II-B.2.

The k_{12}, C_L, and C_M values obtained using full-wave simulations are shown in Fig. 8. k_{12} is calculated using (38) and increases with frequency due to the partial magnetic coupling nature of the filter. C_{Ls} is calculated using (36), and the C_L value between the open ends of the resonator in Fig. (7) is half the value of C_{Ls}.

To obtain the capacitance changes in Fig. 8, the capacitance networks in Fig. 3 and Fig. 6 are realized. The parasitic circuit elements of Fig. 4 were individually found using full-wave simulations. All the capacitance values were first calculated using the area and height of the MEMS or MAM capacitors and then the fringing capacitances and the parasitic inductances were extracted by fitting the circuit model to the full-wave simulation model.

To achieve a capacitance change that covers 4-6 GHz frequency range with continuous step coverage, several simulation steps are needed. First, the C_{sc} values and C_p value are calculated in the equivalent circuit model giving the best step coverage between 4-6 GHz (C_{sw} is fixed due to the fabrication condition of the MEMS device). Then these values are physically realized and simulated using full-wave simulation. The parasitic values such as fringing capacitance and parasitic inductances are extracted with this simulation result, and then the new C_{sc} and C_p are calculated. These steps are repeated until the desired 8 capacitance states are achieved. The equivalent circuit model and full-wave simulation model show a good match at 4-6 GHz. The required C_L values (Fig. 8) are also plotted in Fig. 9 and show that the realized capacitance network covers well the 4.1-5.9 GHz frequency range.

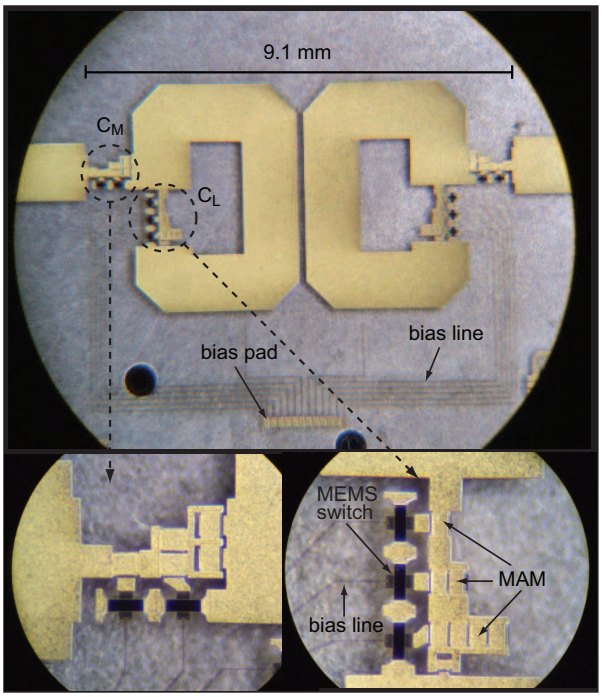

Fig. 10. Fabricated RF-MEMS tunable filter on quartz substrate.

IV. Fabrication and Measurements

The RF-MEMS filter was fabricated on a 0.508 mm quartz substrate (ϵ_r=3.78 and tanδ=0.0001) using a standard RF-MEMS process [7]. The MEMS switch has a 0.3-μm thick bottom Au layer and 0.18 μm Si_3N_4 as a dielectric layer, and

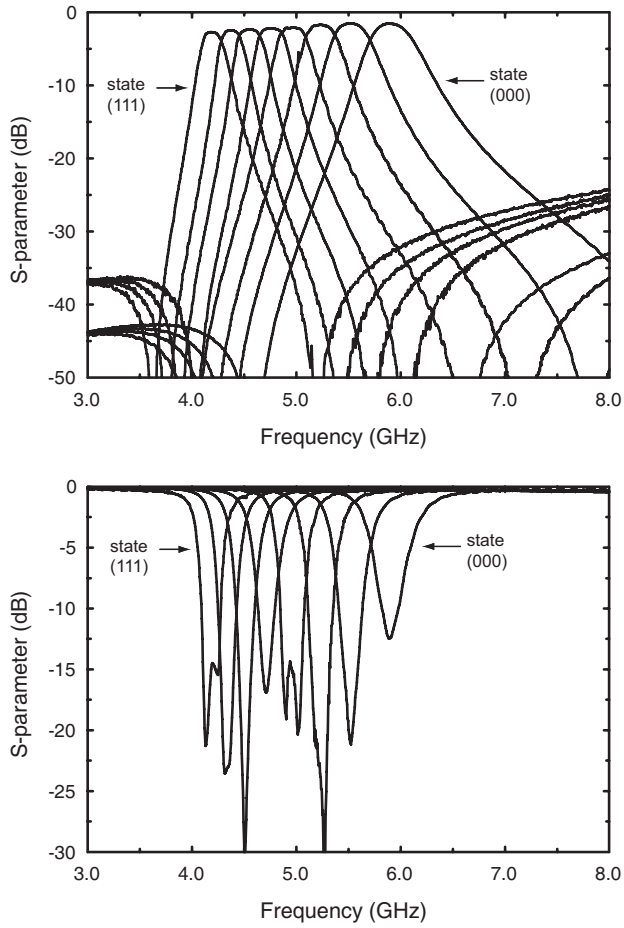

Fig. 11. Measured S_{21} (a) and S_{11} (b) responses of the RF-MEMS tunable filter. S_{22} is nearly identical to S_{11} and is not shown.

the 0.8 μm sputtered gold membrane is suspended 1.4-1.6 μm above the dielectric layer. The bias line is 5 μm wide close to the resonator to minimize the coupling to the electric field and gradually increases to 10-40 μm at the biasing pad. The measured bias line resistance is 8-10 kΩ/sq. The MAM (Metal-Air-Metal) is electroplated to 4 μm thick with an air gap of 1.8 μm (dimensions vary between 50 by 60 to 120 by 120 μm). The average pull-down voltage of the MEMS switch is 50 V (40-70 V) and the corresponding spring constant is 196 N/m (residual stress is 260 MPa). The fabricated RF-MEMS filter and its C_L and C_M capacitance networks are shown in Fig. 10.

The filter was measured in a shielded box which has an opening on one side for the bias probe. The HFSS [12] simulation shows that the radiation loss without shielding is approximately 0.15 dB and is 0.05 dB with the shielding box (Fig. 13). The SOLT calibration was done up to the outside connector. The measured S-parameters are shown in Fig. 11. The measured filter covers 4.17 GHz to 5.91 GHz with continuous coverage and 2 to 3 dB crossovers. The measured insertion loss and 1-dB bandwidth at 4.17-5.91 GHz are 2.75-1.53 dB and 4.0-4.7 %, respectively. The fitted Q is 85 at 4.17 GHz and increases to 170 at 5.91 GHz. The measured S_{11} shows an excellent match ($>$ 15 dB) over the entire tuning

TABLE I
MEASURED 8 STATES OF THE RF-MEMS FILTER.

state	111	011	101	001	110	010	100	000
f_0 (GHz)	4.17	4.38	4.56	4.76	4.97	5.24	5.53	5.91
I.L.(dB)	2.75	2.45	2.37	2.22	2.07	1.73	1.53	1.53
1-dB BW(%)	4.0	4.1	4.4	4.5	4.7	4.6	4.6	4.7
1-dB BW(MHz)	167	180	201	214	234	241	254	278

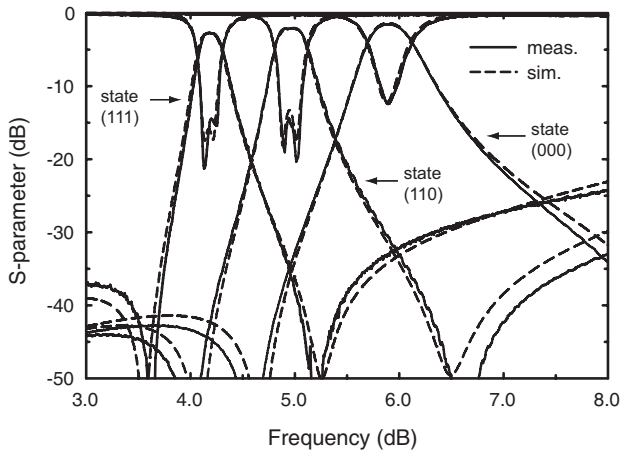

Fig. 12. Measured and simulated responses of the RF-MEMS tunable filter.

range except the highest frequency state ($\backsim$ 12 dB), and this is due to one un-actuated switch in C_M. The measured results are summarized in Table I.

The measured and simulated results are plotted in Fig. 12 for states (000), (110), and (111). The simulation results are obtained by combining the full-wave model of the coupled resonators (Fig. 7) with the model of the capacitance networks. The simulated response is identical with either the equivalent circuit capacitance model or with the full-wave capacitance model and the results are 30-80 MHz lower than the measured values. The fabricated Si_3N_4 has a dielectric constant of 6-9

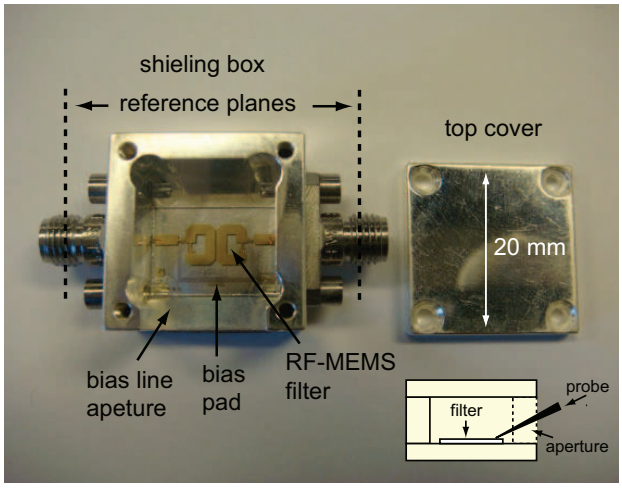

Fig. 13. RF-MEMS filter in the shielding box.

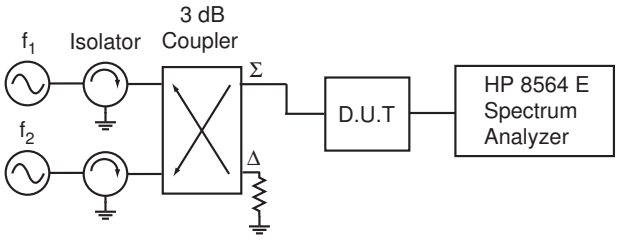

Fig. 14. Experimental setup for intermodulation measurements.

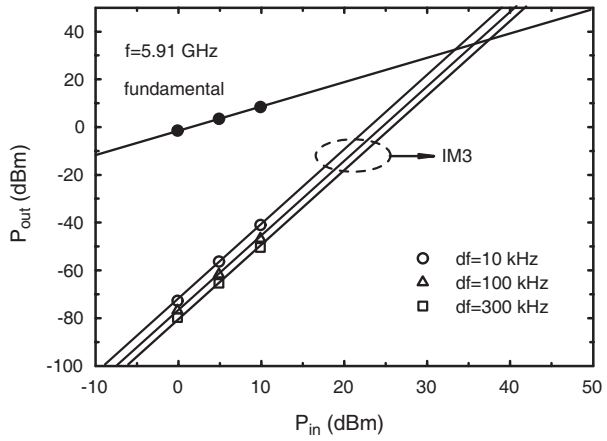

Fig. 15. Measured IM-products of the RF-MEMS tunable filter.

depending on the fabrication conditions and in the original simulation model, the dielectric constant is assumed to be 4.0 due to the roughness of the surface [13]. The simulations in Fig. 12 are therefore done with a dielectric constant of 3.75 (instead of 4.0) and show excellent agreement with measurements.

The resonator with 4 μm plating thickness and 1.2 mm width is simulated using Sonnet and the intrinsic Q simulated is 210-245 at 4-6 GHz. This is much higher than the fitted Q of 85-170 and is due to the effected series resistance of the C_L network (R_s=0.9 Ω fitted). The series resistance of C_L is mostly from the thin bottom metal layer (0.3 μm) which is only 0.2-0.25 skin depth thick at 4-6 GHz. A 0.3 μm metal thickness was used for good step coverage in the bridge membrane. If the thickness of the bottom metal layer is increased to 0.6 μm, the series resistance becomes 0.45 Ω, and the overall Q of the loaded resonator increases to 125-210 resulting in an insertion loss of 1.75-1.10 dB at 4-6 GHz.

A. Nonlinear Characterization of the RF MEMS Filter

The nonlinear characterization was done using the experimental setup in Fig. 14. The measurement was done on the highest frequency state where all the MEMS switches are in the up-state position and with the highest filter Q and this results in the worst IM_3 products (Fig. 15). Measurements show that the IIP_3 is $>$ 37 dBm for $\Delta f >$ 300 kHz. For the RF-MEMS switches, the intermodulation component follows the mechanical response of the bridge, and the IIP_3 level drops by 40 dB/decade for $\Delta f > f_0$ ($f_0 \sim$ 180 kHz). At Δf=1 MHz, the IIP3 is 57 dBm and this is the limit of our measurement setup.

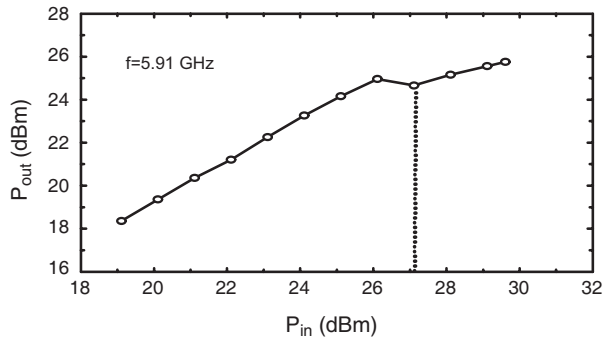

Fig. 16. Measured P-1dB of the RF-MEMS tunable filter.

The power handling capability of the filter was investigated by measuring the P-1dB of the filter (Fig. 16). The measurement was also done in the highest frequency state and maximum filter Q. One of the switches was actuated down around 27 dBm and this results in a frequency shift and a 3 dB power loss. Simulations show that an RF power of 0.5-1.0 W results in an RF rms voltage of 30-40 V at C_{sw3}, and this is enough to move switch and distort the filter response.

V. Conclusion

Low-loss tunable filter with 3-bit high-Q Orthogonal RF-MEMS capacitance network were designed, fabricated, and measured. The lossy coupling between the resonant electric field and the bias lines in the multi-bit RF-MEMS capacitance network were analyzed and the orthogonal capacitance network design was suggested to minimize the lossy coupling. The Q of the measured filter is 85-170 at 4-6 GHz and this is a state-of-the-art result. The Q can be enhanced to 125-210 with the use of a thicker bottom electrode (0.6 μm). A suspended resonator design with small loading capacitance values (X_C $>$ j300 Ω) can result in a filter Q up to 300 and this is being done at UCSD.

References

[1] W. J. Keane, "YIG filters aid wide open receivers," *Microwave J.*, vol. 17, no. 8, Sept. 1980.

[2] I. C. Hunter and J. D. Rhodes, "Electronically tunable microwave bandpass filters," *IEEE Trans. Microwave Theory & Tech.*, vol. 30, no. 9, pp. 1354–1360, Sept. 1982.

[3] A. R. Brown and G. M. Rebeiz, "A varactor-tuned RF filter," *IEEE Trans. Microwave Theory & Tech.*, vol. 48, no. 7, pp. 1157–1160, July 2000.

[4] M. Sanchez-Renedo, R. Gomez-Garcia, J. I. Alonso, and C. Briso-Rodriguez, "Tunable combline filter with continuous control of center frequency and bandwidth," *IEEE Trans. Microwave Theory & Tech.*, vol. 53, no. 1, pp. 191–199, Jan. 2005.

[5] A. Pothier, J.-C. Orlianges, G. Zheng, C. Champeaux, A. Catherinot, P. B. D. Cros, and J. Papapolymerou, "Low-loss 2-bit tunable bandpass filters using MEMS DC contact switches," *IEEE Trans. Microwave Theory & Tech.*, vol. 53, no. 1, pp. 354–360, Jan. 2005.

[6] B. Pillans, A. Malczewski, R. Allison, and J. Brank, "6-15 GHz RF MEMS tunable filters," in *IEEE MTT-S Int. Microwave Symp. Dig.*, Long Beach, CA USA, June 2005, pp. 919–922.

[7] K. Entesari and G. M. Rebeiz, "A differential 4-bit 6.5-10 GHz RF MEMS tunable filter," *IEEE Trans. Microwave Theory & Tech.*, vol. 53, no. 3, pp. 1103–1110, Mar. 2005.

[8] S.-J. Park, K.-Y. Lee, and G. M. Rebeiz, "Low-loss 5.15-5.70-GHz RF MEMS switchable filter for wireless LAN applications," *IEEE Trans. Microwave Theory & Tech.*, vol. 54, no. 11, pp. 3931–3939, Nov. 2006.

[9] L. Dussopt and G. M. Rebeiz, "Intermodulation distortion and power handling in RF MEMS switches, varators, and tunable filters," *IEEE Trans. Microwave Theory & Tech.*, vol. 51, no. 4, pp. 1247–1256, Apr. 2003.
[10] J. S. Hayden and G. M. Rebeiz, "Very low loss distributed X-band and Ka-band mems phase shifters using metal-air-metal capacitors," *IEEE Trans. Microwave Theory & Tech.*, vol. 51, no. 1, pp. 309–314, Jan. 2003.
[11] *Sonnet 10.52*, Sonnet Software, Inc., North Syracuse, NY USA, 2005.
[12] *HFSS 10.1*, Ansoft, Corporation., Pittsburgh, PA USA, 2006.
[13] G. M. Rebeiz, *RF MEMS Theory, Design, and Technology*. New York, USA: Wiley, 2003.

Sang-June Park received the B.S. degree in physics from Youngnam University, Kyungsan, Korea, in 1991, the M.S. degree in electrical engineering from The University of Michigan at Ann Arbor, in 2004, and is currently working toward the Ph.D. degree in electrical engineering (with an emphasis on applied electromagnetics and RF circuits) at The University of Michigan at Ann Arbor. In 1997 he joined Samsung-Electromachanics R&D Center and involved in the development of Microwave Ceramic Filters and LTCC Antenna Switch Modules. His current research includes RF MEMS for microwaves and millimeter-wave applications, microwave tunable filters and antenna.

Gabriel M. Rebeiz Gabriel M. Rebeiz is a Professor of electrical engineering at the University of California, San Diego. He has contributed to planar mm-wave and THz antennas and imaging arrays, RF MEMS and mm-wave RFICs. He is the author of the book, RF MEMS: Theory, Design and Technology, Wiley (2003). He is an IEEE Fellow, an NSF Presidential Young Investigator, an URSI Koga Gold Medal Recipient, an IEEE MTT Distinguished Young Engineer (2003), a recipient of the IEEE MTT 2000 Microwave Prize, and received the 1998 Amoco Teaching Award given to be best undergraduate teacher at the University of Michigan. He is the Director of the UCSD/NEU DARPA S&T Center on RF MEMS.

PLACE PHOTO HERE

Mohammed A. El-tanani Mohammed A. El-tanani

PLACE PHOTO HERE

Isak Reines Isak Reines

Mini-MEMS 4-State Bandstop Filter

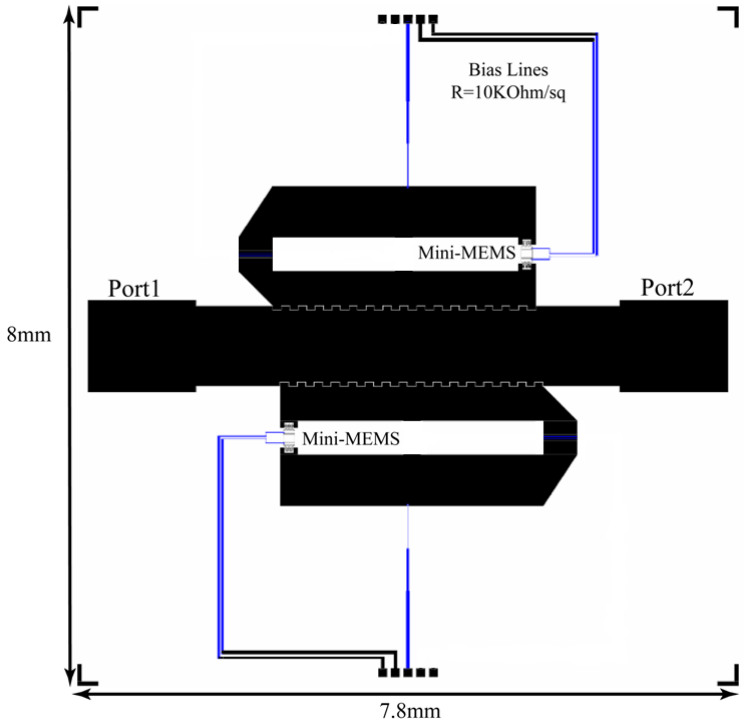

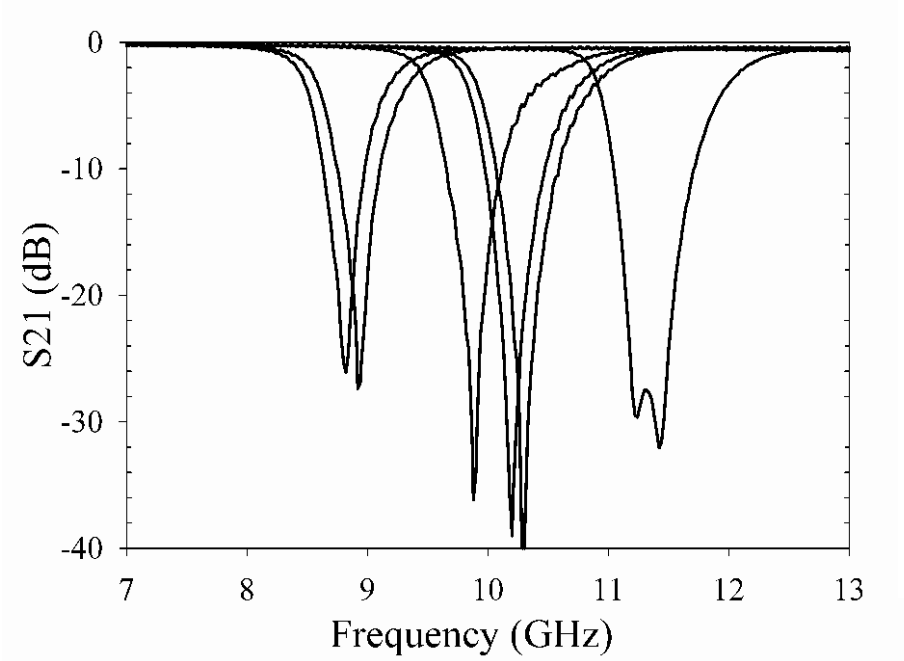

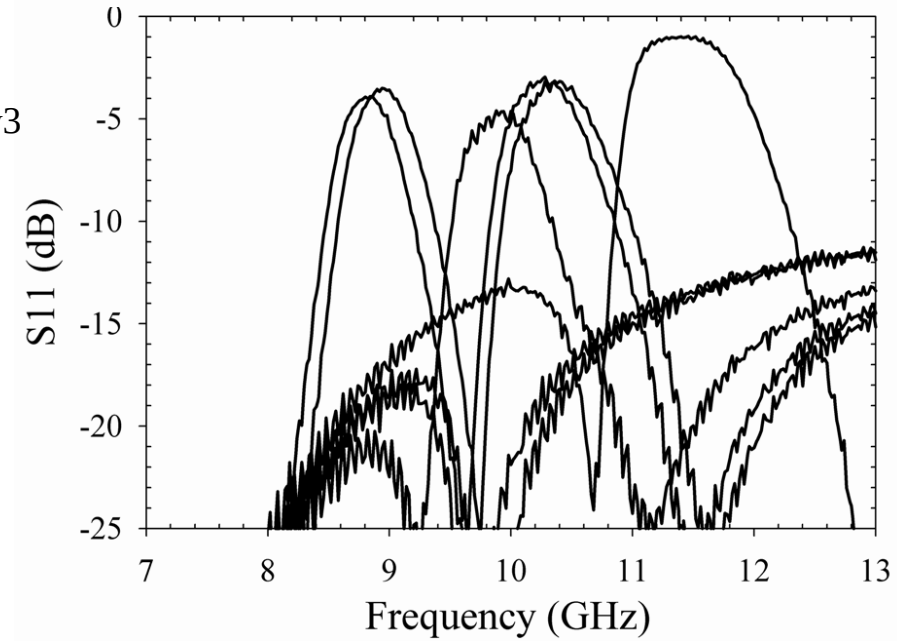

- Resonator loaded with back to back 3by2 and 3by3 arrays of Mini-MEMS (4-states)
- Some analogue tuning is shown here
- Switchable from 8.82 GHz – 11.32 GHz
- 2.5 GHz Tuning range
- Minimum Rejection = 26.2 dB
- Max. insertion loss at 7 & 13 GHz

  = 0.197dB and 0.607 dB respectively (includes coax-microstrip connector loss)

IIP3 Measurement Setup

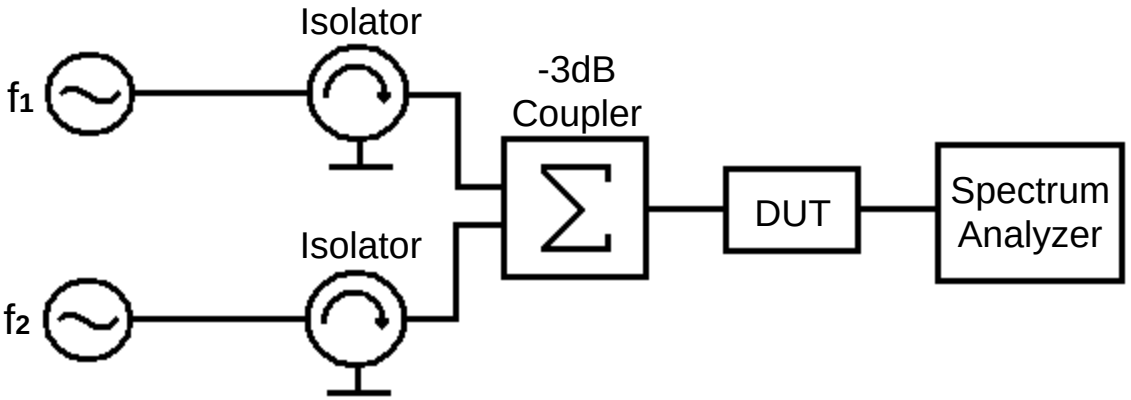

- Measurements were taken from the 4-state filter shown below

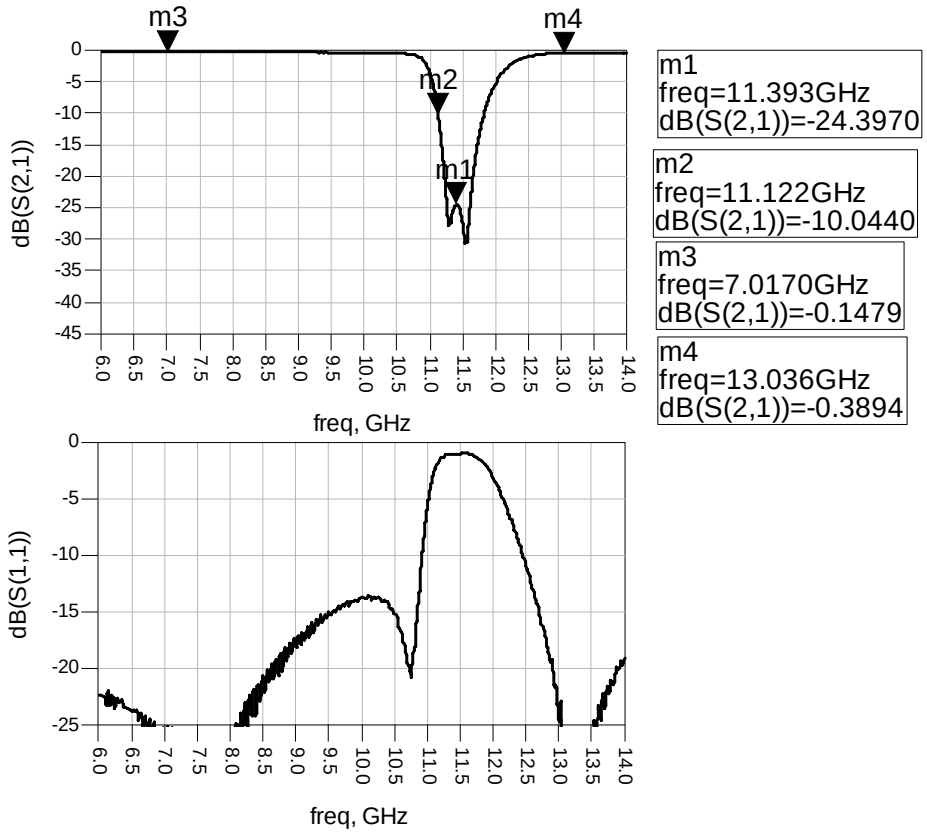

IIP3 Measurements

fo =11.412 GHz (Null), f=1MHz

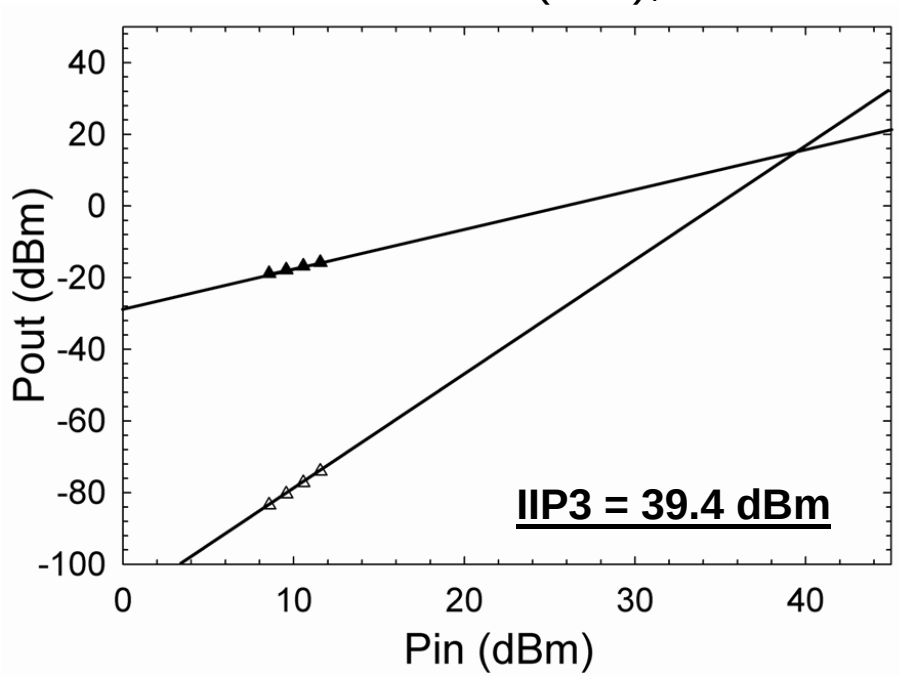

fo =11.112 GHz (-10 dB on Null), f=1MHz

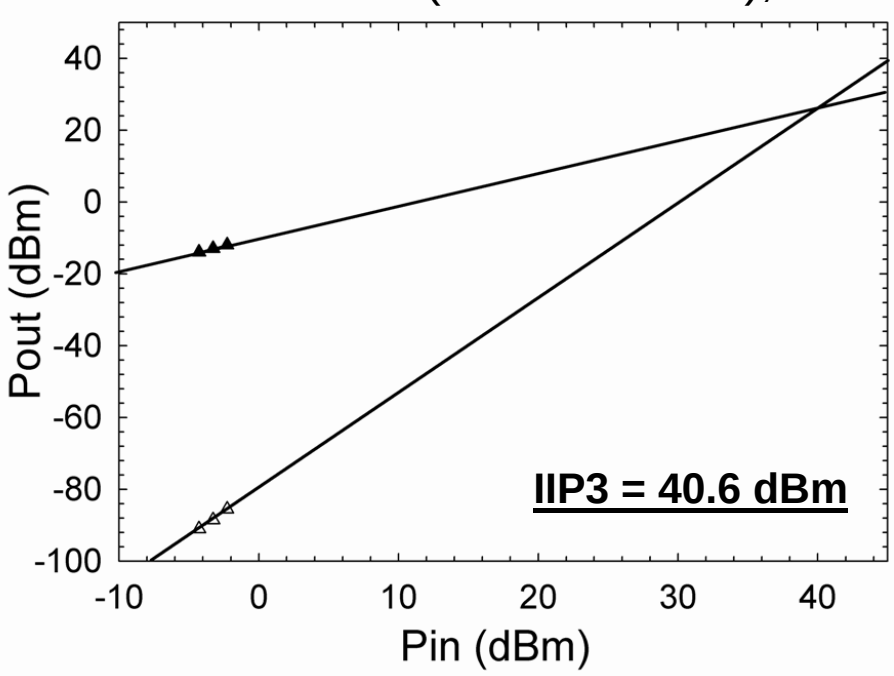

Agilent E4448A Spectrum Analyzer Settings

- Input Attenuation = 16dB
- Reference level = 0 dB
- Resolution BW = 3.9 kHz
- Span = 4 MHz
- Averaging 100 sweeps

- Max input power to Spectrum analyzer is -10dBm before mixer distortion is visible
- Spectrum Analyzer IIP3 ~45dBm with attenuation =16dB
- I couldn't measure any intermodulation distortion at 7 and 13 GHz while keeping power into spectrum analyzer less than -10dBm

Filter Power Handling Simulations

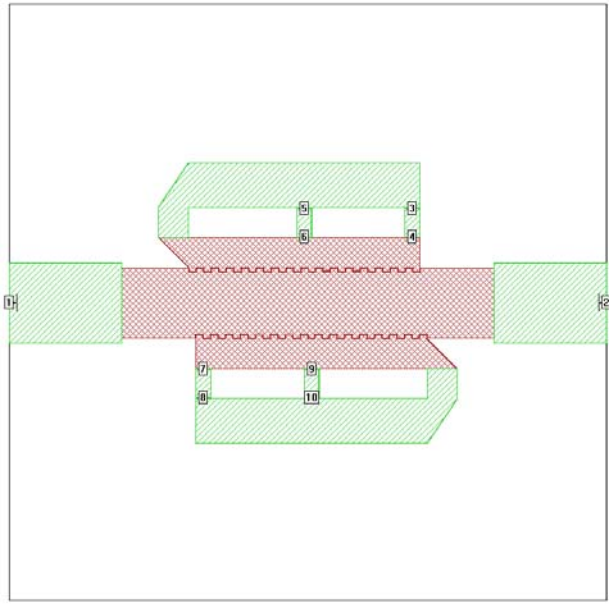

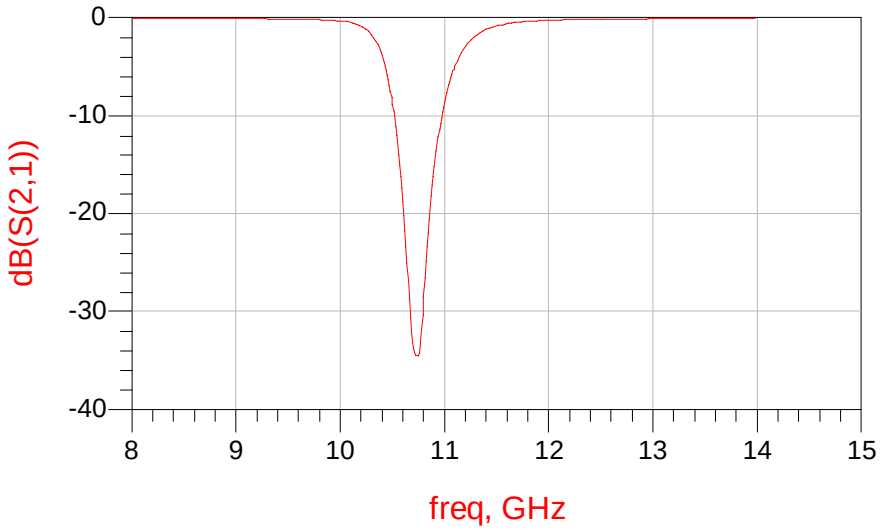

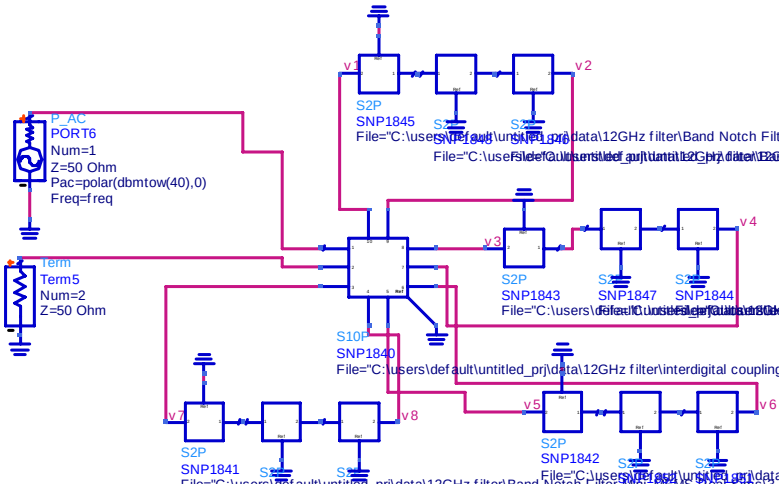

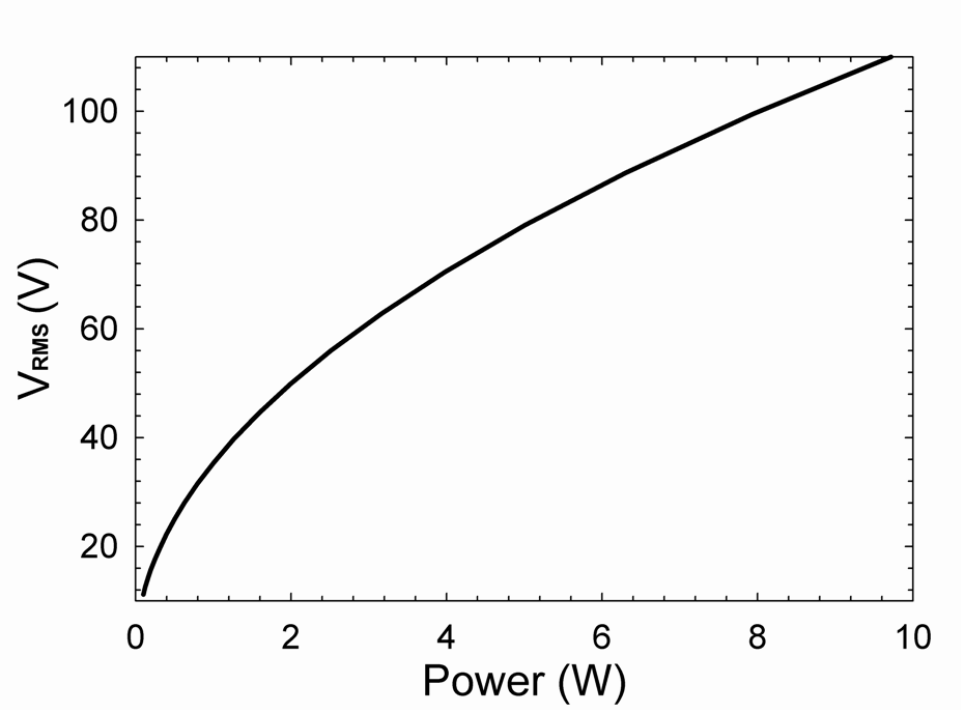

Filter Power Measurements

Measurement Setup

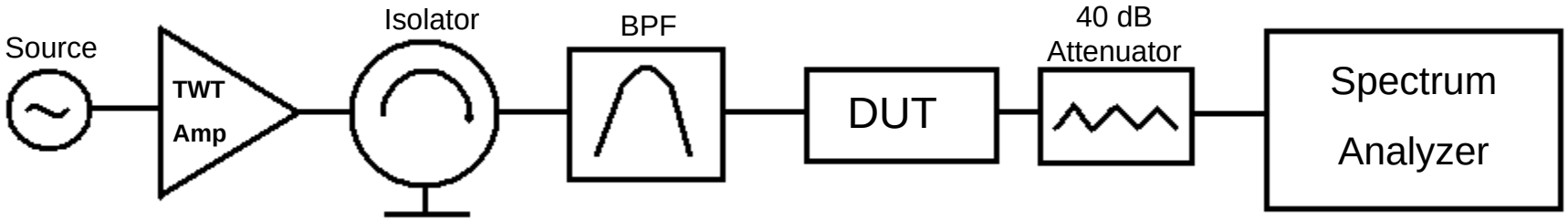

fo = 11.412 GHz

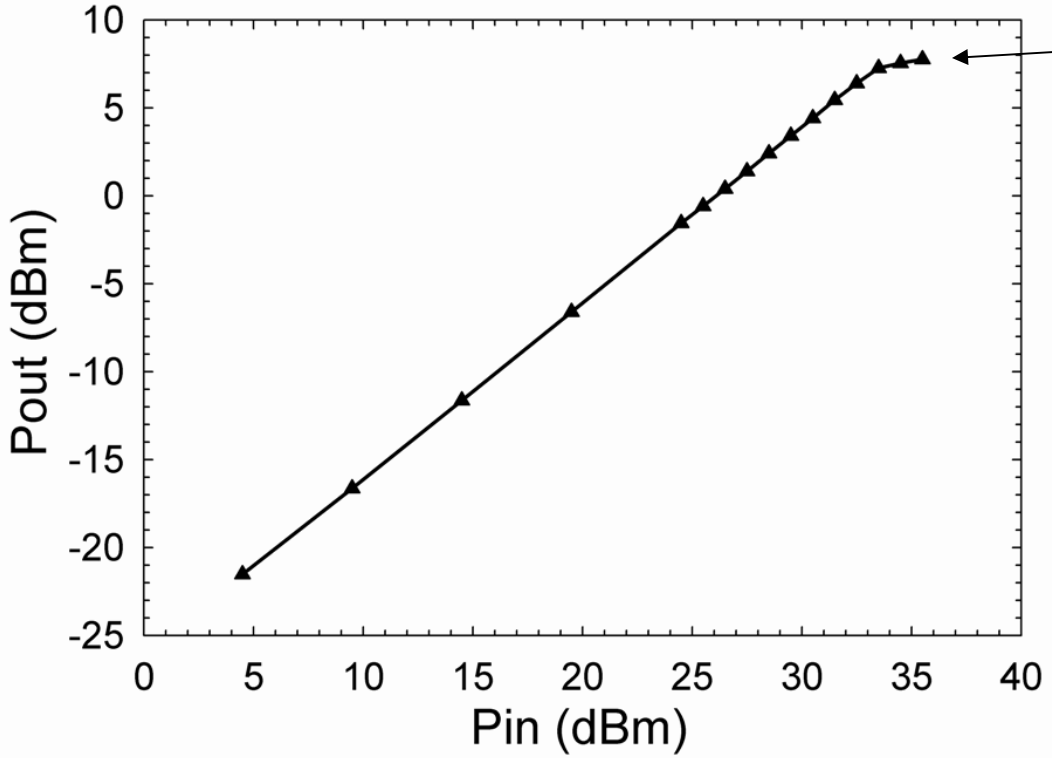

Pout dropping as Null moves and rejection increases from initial M1 marker at 11.412 GHz

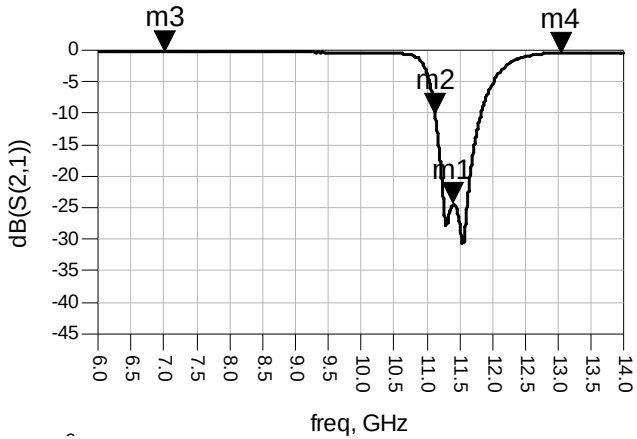

Detailed Layout of the 4-6 GHz RF MEMS Filter

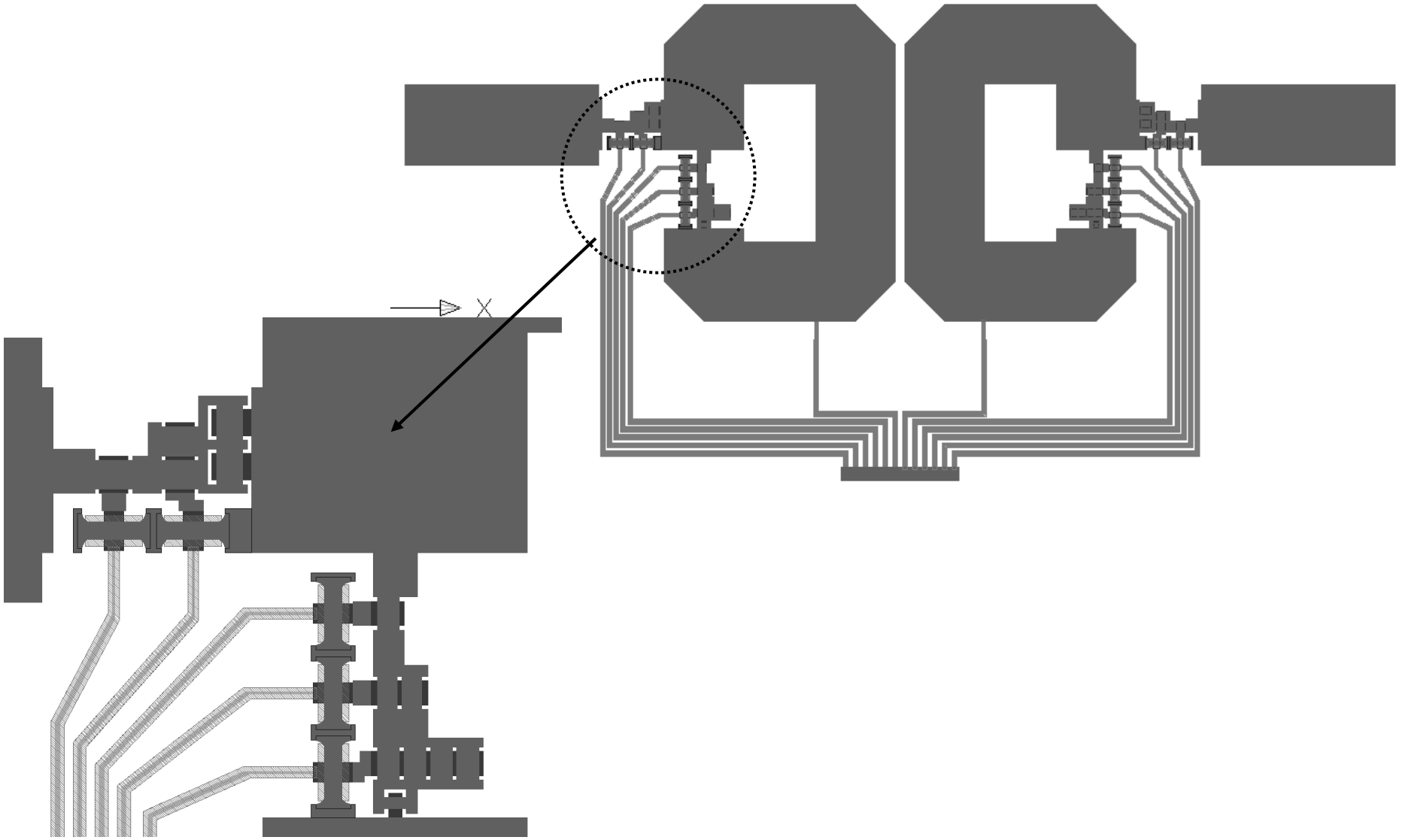

Fabricated Filter

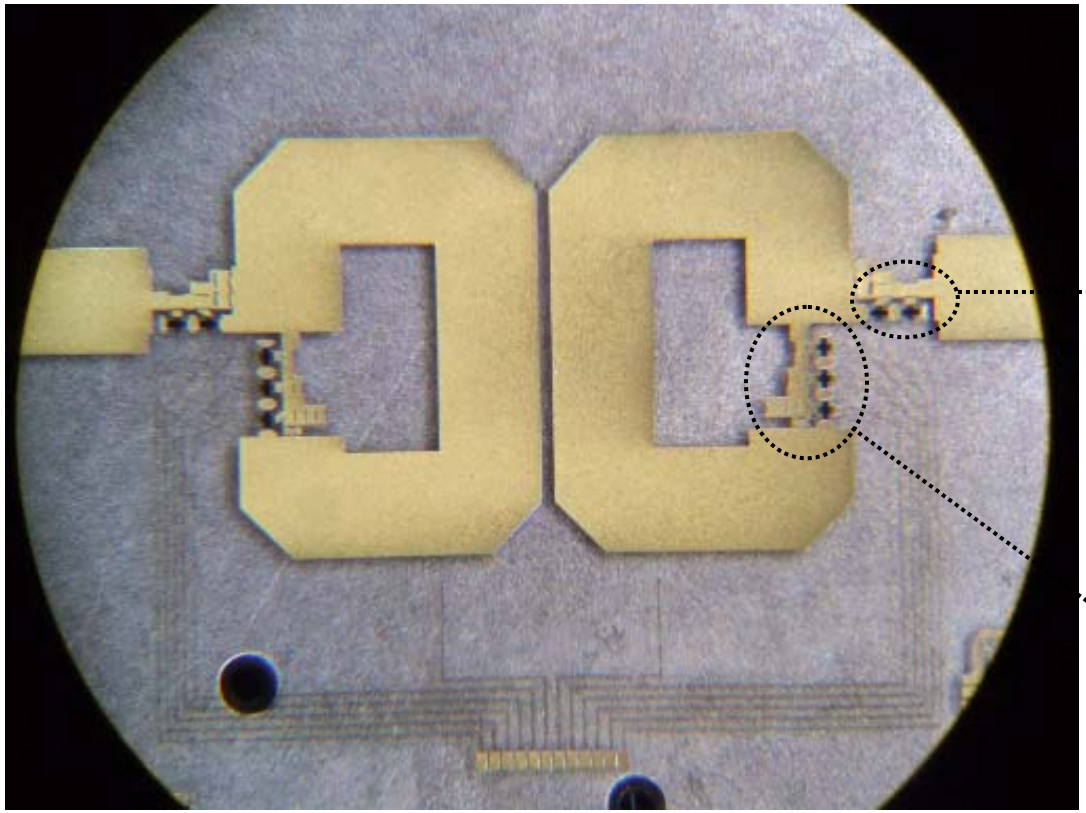

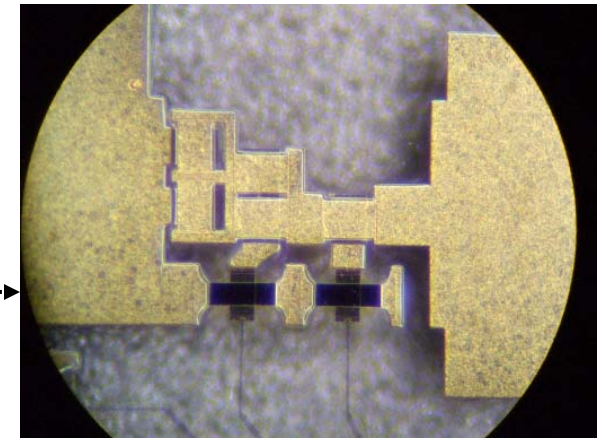

2-bit CM

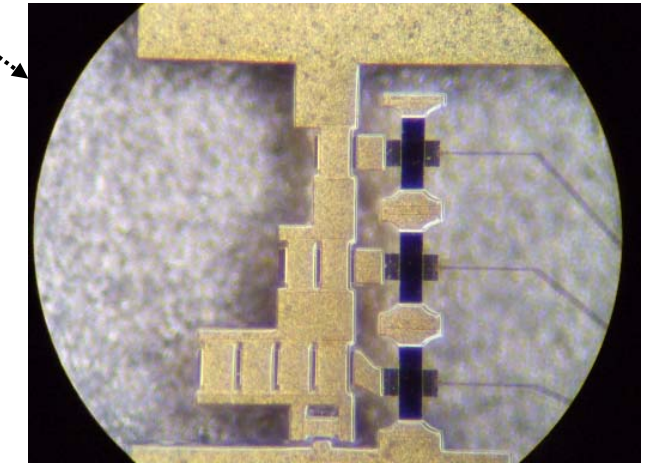

3-bit CL

MEASURED RESULTS..this is not a simulation..these are measured!

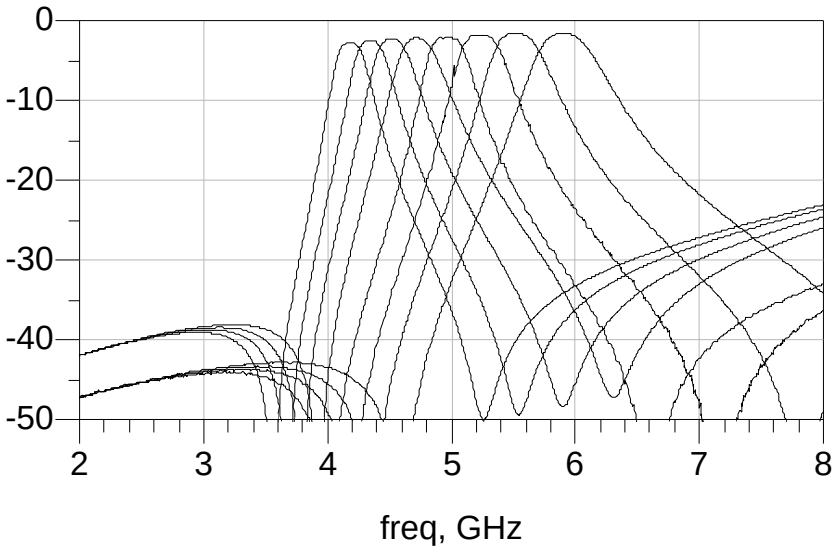

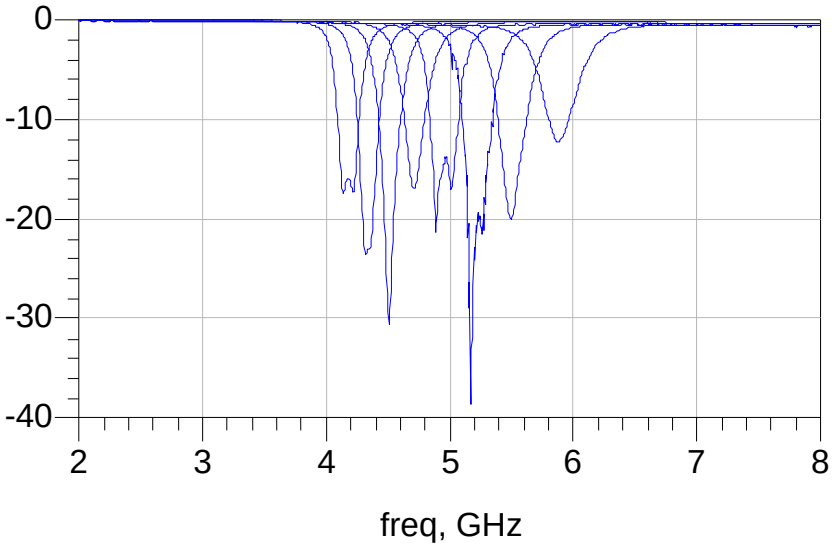

states	**1**	2	3	4	**5**	**6**	**7**	**8**
f (GHz)	**4.18/4.15**	4.37/4.30	4.56/4.47	4.75/4.64	**4.97/4.95**	**5.24/5.21**	**5.53/5.50**	**5.91/5.85**
-1dB BW (%)	**4.0/4.2**	4.0/4.1	4.1/4.3	4.1/4.3	**4.7/4.7**	**4.6/4.6**	**4.6/5.2**	**4.7/5.1**
I.L. (dB)	**2.73/2.09**	2.44/1.84	2.26/2.10	2.17/1.80	**2.07/1.86**	**1.73/1.56**	**1.53/1.46**	**1.53/1.08**
CL (fF)	CLddd	CLudd	CLdud	CLuud	**CLddu**	**CLudu**	**CLduu**	**CLuuu**
CM (fF)	CMxd\CMdd		CMxd\CMud		**CMux\CMdu**		**CMux\CMuu**	

voltage across the MEMS switches

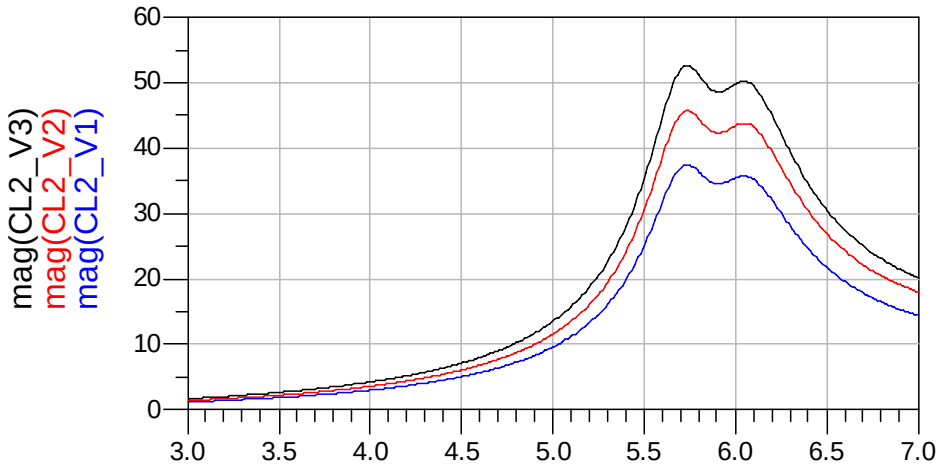

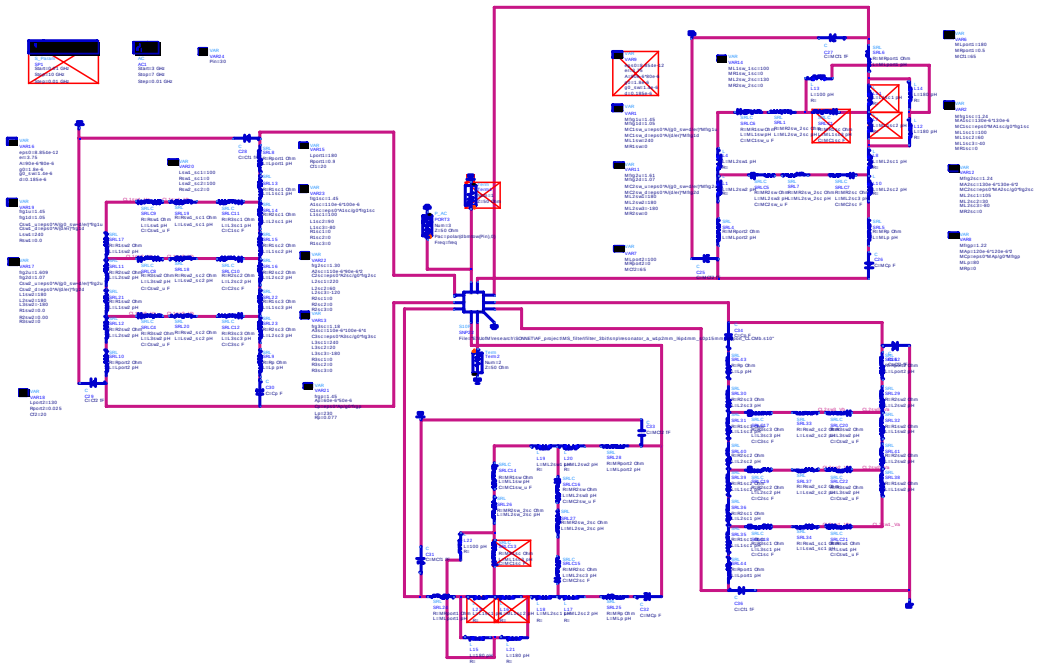

max voltage across the MEMS switch with 1 W input power
➔ 53 V

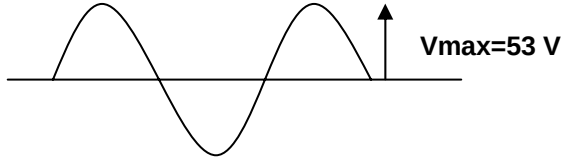

MEMS pull in voltage: Vp=60-90 V (3 kHz square wave)